Acta Biomaterialia 8 (2012) 878–885

Contents lists available at SciVerse ScienceDirect

Acta Biomaterialia

journal homepage: www.elsevier.com/locate/actabiomat

Effects of structural properties of electrospun TiO_2 nanofiber meshes on their osteogenic potential

Xiaokun Wang [a,1], Rolando A. Gittens [b,c,1], Rosemary Song [d], Rina Tannenbaum [b], Rene Olivares-Navarrete [d], Zvi Schwartz [c,d], Haifeng Chen [a], Barbara D. Boyan [b,c,d,*]

[a] Department of Biomedical Engineering, Peking University, Beijing 100871, China
[b] School of Materials Science and Engineering, Georgia Institute of Technology, Atlanta, GA, USA
[c] Institute for Bioengineering and Bioscience, Georgia Institute of Technology, Atlanta, GA, USA
[d] Wallace H. Coulter Department of Biomedical Engineering at Georgia Tech and Emory University, Georgia Institute of Technology, Atlanta, GA, USA

ARTICLE INFO

Article history:
Received 20 July 2011
Received in revised form 21 September 2011
Accepted 17 October 2011
Available online 31 October 2011

Keywords:
Nanostructures
Electrospinning
Scaffold
Titanium implant
Tissue engineering

ABSTRACT

Ideal outcomes in the field of tissue engineering and regenerative medicine involve biomaterials that can enhance cell differentiation and production of local factors for natural tissue regeneration without the use of systemic drugs. Biomaterials typically used in tissue engineering applications include polymeric scaffolds that mimic the three-dimensional structural environment of the native tissue, but these are often functionalized with proteins or small peptides to improve their biological performance. For bone applications, titanium implants, or more appropriately the TiO_2 passive oxide layer formed on their surface, have been shown to enhance osteoblast differentiation in vitro and to promote osseointegration in vivo. In this study we evaluated the effect on osteoblast differentiation of pure TiO_2 nanofiber meshes with different surface microroughness and nanofiber diameters, prepared by the electrospinning method. MG63 cells were seeded on TiO_2 meshes, and cell number, differentiation markers and local factor production were analyzed. The results showed that cells grew throughout the entire surfaces and with similar morphology in all groups. Cell number was sensitive to surface microroughness, whereas cell differentiation and local factor production was regulated by both surface roughness and nanofiber diameter. These results indicate that scaffold structural cues alone can be used to drive cell differentiation and create an osteogenic environment without the use of exogenous factors.

1. Introduction

The decade from 2001 to 2011 has been termed the "bone and joint decade", because it has been recognized that musculoskeletal injuries are the most reported health condition in the USA, with an associated cost close to 8% of the US gross domestic product in lost wages and healthcare-related costs [1]. More than 25% of musculoskeletal injuries involve bone fractures, with many of these fractures not being able to heal by themselves, thus requiring some type of bone void filler that can promote bone regeneration and reduce the healing time for the patient. With an aging population in developed countries and statistics showing, for example, that one in every two women over 50 years old will suffer an osteoporotic bone fracture [2], there is a pressing need to find reliable bone repair materials.

Tissue engineering offers a promising approach for repair and regeneration of damaged human tissue by mimicking the extracellular environment and taking advantage of the natural cues cells use to perform their role. A common methodology for bone tissue engineering is the fabrication of three-dimensional (3-D) porous scaffolds, which allow cells to invade the construct in vitro or in vivo and more closely mimic the native environment [3,4]. There are several methods to prepare porous scaffolds, such as freeze-drying and salt-leaching methods for polymer scaffolds [5], and replica methods used in ceramics [3,6]. Although discovered over 100 years ago [7], electrospinning has gained popularity recently as a simple and versatile method to produce fibrous structures from synthetic and natural polymers with nano- to microscale dimensions [7,8].

The electrospinning process has been extensively applied to create nanofiber scaffolds for cardiovascular [9], urologic [10] and bone tissue engineering applications [11], among others, using synthetic organic polymers such as poly(ε-caprolactone) [12] and

* Corresponding author. Address: Institute for Bioengineering and Bioscience, Georgia Institute of Technology, 315 Ferst Drive, NW (Suite 1108), Atlanta, GA 30332-0363, USA. Tel.: +1 404 385 4108; fax: +1 404 894 2291.
E-mail address: barbara.boyan@bme.gatech.edu (B.D. Boyan).
[1] Joint first authors.

1742-7061/$ - see front matter © 2011 Acta Materialia Inc. Published by Elsevier Ltd. All rights reserved.
doi:10.1016/j.actbio.2011.10.023

poly(lactide-co-glycolide) [13]. Natural polymers such as collagen [14] and silk fibroin [15] have also been used in the electrospinning setup. Electrospun scaffolds have also been made using a composite of synthetic and natural polymers to take advantage of the mechanical properties of the former and the biological performance of the latter [16,17]. An attractive property of organic polymers is that they can be resorbed by the body and fully replaced by the native tissue [18]. These organic polymers can also provide surfaces for cell attachment and growth, but it is often necessary to functionalize them, specifically for bone applications, with osteogenic molecules such as hydroxyapatite [11] and growth factors like bone morphogenic proteins [19] to promote cell differentiation.

Ceramic scaffolds have also been considered as bone graft substitutes for bone repair, with calcium-based chemistries such as hydroxyapatite [20] and β-tricalcium phosphate [21] commonly used because of their bioactivity and, in some cases, tunable resorbability [3]. Studies using solid substrate surfaces show that cell differentiation is sensitive to microscale and nanoscale topography [22–26]. When osteoblasts or mesenchymal stem cells are cultured on titanium substrates, which have an inherent TiO_2 ceramic layer on the surface, they exhibit enhanced osteoblastic differentiation, particularly if the surface has both microscale and nanoscale features [27–29]. Although not bioresorbable, TiO_2 could serve as an attractive substrate for bone tissue engineering due to its good biological performance. Whether surface structure also plays a role when cells are growing on TiO_2 nanofiber meshes is not known. The purpose of this study was to assess the contributions of nanofiber dimensions and microscale pattern on cell response. To do this, pure TiO_2 nanofiber meshes were fabricated using electrospinning to have different surface microroughness and nanofiber diameters.

2. Materials and methods

2.1. Preparation and characterization of TiO_2 scaffolds

Titania nanofiber meshes were prepared from a TiO_2 gel solution prepared by hydrolysis of titanium(IV) isopropoxide (TiP) in poly(vinyl pyrrolidone) (PVP, $M_w \approx 300{,}000$) and acetic acid. Initially, 0.5 ml of TiP was mixed with 0.5 ml ethanol, with 0.5 ml acetic acid used as catalyst. After stirring for 10 min, the solution was added to 1.5 ml of 6% PVP or 10% PVP in ethanol solution and magnetically stirred for 30 min. To produce electrospun nanofiber meshes, 1 ml of the hybrid solution was loaded into a plastic syringe with a blunt-ended stainless steel needle. The nanofibers were spun using a feeding rate of 0.5 ml h^{-1}, a collection distance of 10 cm and an applied voltage of 8 kV. To create a microscale pattern, the electrospun fibers were collected on a cross-hatched bronze net to imprint a pattern on the side of the mesh in contact with the collector. The PVP was removed from the fibers by heating in air at 700 °C for 3 h on top of Si wafers, and all samples were sterilized under ultraviolet (UV) irradiation for at least 12 h before characterization or cell experiments.

Sample topography and cell morphology were examined by scanning electron microscopy (SEM; Ultra 60 FEG-SEM, Carl Zeiss SMT Ltd., Cambridge, UK) using a 5 kV accelerating voltage and 30 μm aperture. Fiber dimensions and pore sizes were evaluated using image analysis software (ImageJ, NIH software) from three images of two different samples. Fiber diameter was evaluated at ×20,000 magnification and pore size at ×5000, with at least 100 fibers and 200 pores per mesh determined manually and analyzed by the software.

The chemical composition of the scaffolds was examined by energy-dispersive X-ray spectroscopy (EDX; INCA EDX, Thermo Fisher Scientific, West Palm Beach, FL), with two different scaffolds per group analyzed in at least three different sites. Additionally, surface atomic concentrations were obtained from two specimens per group, two spots per specimen, by X-ray photoelectron spectroscopy (XPS; Thermo K-Alpha XPS, Thermo Fisher Scientific, West Palm Beach, FL). The instrument was equipped with a monochromatic Al K_α X-ray source ($h\nu$ = 1468.6 eV) and spectra were collected using an X-ray spot size of 400 μm and a pass energy of 200 eV, with 1 eV increments, at a 55° takeoff angle.

Surface roughness of the porous TiO_2 meshes was evaluated using laser confocal microscopy (LCM; Lext LCM, Olympus, Center Valley, PA). LCM analyses were performed over a 644 μm × 644 μm area using a scan height step of 50 nm, a ×20 objective and a cutoff wavelength of 100 μm. Three scans each of at least two different samples per group were analyzed. The roughness parameters determined were mean surface roughness (S_a) and peak-to-valley height (S_z), and topographical images were also collected at the ×20 magnification.

Finally, crystal structure X-ray diffraction (XRD) was investigated using 1.8 kW Cu K_α radiation, a 1° parallel plate collimator, a 0.25 divergence slit and a 0.04 rad soller slit (X'Pert PRO Alpha-1 diffractometer, PANalytical, Almelo, The Netherlands). Two samples per group were analyzed.

2.2. Cell culture

MG63 cells (American Type Culture Collection, Rockville, MD) were cultured in Dulbecco's modified Eagle's medium (DMEM; Cellgro® by Mediatech, Inc., Manassas, VA), containing 10% fetal bovine serum (Gibco, Carlsbad, CA) and 1% penicillin–streptomycin (Gibco) at 37 °C in 5% CO_2 and 100% humidity. The MG63 cell line was originally derived from a human osteosarcoma and has been shown to exhibit many characteristics of pre-mature osteoblasts, making it an attractive model for in vitro studies [30–32]. Cells were grown on 24-well plate tissue culture polystyrene (TCPS) using a seeding density of 20,000 cells $well^{-1}$. Alternatively, cells were seeded onto two different formulations of the TiO_2 meshes (6% and 10% PVP), on both their flat and patterned sides, after UV sterilization overnight. The meshes were slightly large to fit in a 24-well plate, so larger well plates had to be used to avoid damage. Meshes were initially seeded in an untreated 6-well plate using a volume of 150 μl containing 20,000 cells to cover just the surface of the sample, and incubated for 4 h to allow for initial cell attachment. Next, each well was brought up to a final volume of 2 ml and incubated for an additional 20 h. After the first 24 h, TiO_2 meshes were transferred to an untreated 12-well plate containing 1 ml of medium in each well. MG63 cells were fed every 48 h until confluent on the TCPS. Cells in all wells were then incubated with fresh medium for 24 h and harvested. Conditioned media were collected as described below. Cell layers were washed twice with DMEM, followed by two sequential incubations in 500 μl of 0.25% trypsin–ethylenediaminetetraacetic acid (Gibco) for 10 min at 37 °C to ensure all cells were released from their substrate. Cells were then centrifuged at 670 × g for 15 min, resuspended in 10 ml of saline solution and counted with a Z1 Coulter particle counter (Beckman Coulter, Brea, CA). Cells were centrifuged again at 670 × g for 15 min, the supernatant was decanted and the cell pellets were resuspended in 500 μl of 0.05% Triton-X-100. Cells were lysed by sonication.

2.3. Biochemical assays

Cell differentiation was evaluated as a function of alkaline phosphatase specific activity as an early differentiation marker, and osteocalcin content in the conditioned media as a late differentiation marker, as previously described [29]. Alkaline phosphatase specific activity was assayed as the release of p-nitrophenol from

p-nitrophenylphosphate at pH 10.2 [33,34], and values were normalized to the protein content, which was detected as colorimetric cuprous cations in a bicinchoninic reaction (BCA Protein Assay Kit, Pierce Biotechnology Inc., Rockford, IL, USA) at 570 nm (Microplate Reader, BioRad Laboratories Inc., Hercules, CA, USA) [35]. Osteocalcin levels in the conditioned media were measured with a commercially available radioimmunoassay kit (Human Osteocalcin RIA Kit, Biomedical Technologies, Stoughton, MA) using an LS1500 gamma counter (Beckman Coulter, Brea, CA) as described previously [36].

The conditioned media were also assayed for protein levels of growth factors and cytokines, as described previously [37,38]. Osteoprotegerin (OPG), a cytokine that works as a decoy receptor for the receptor activator for nuclear factor κB ligand to inhibit osteoclastogenesis, was measured using an enzyme-linked immunosorbent assay (ELISA) kit (DY805 Osteoprotegerin DuoSet, R&D Systems, Minneapolis, MN). Vascular endothelial growth factor (VEGF), a growth factor involved in vasculogenesis and angiogenesis, was also measured using an ELISA kit (DY293B VEGF DuoSet, R&D Systems).

2.4. Statistical analysis

Data from characterization of the TiO_2 meshes are presented as the mean ± one standard deviation (SD) of all the measurements performed on different samples. Data from cell experiments are presented as mean ± standard error (SE) for six independent cultures. All experiments were repeated at least twice to ensure validity of the observations and results from individual experiments are shown. Data were evaluated by analysis of variance, and significant differences between groups were determined using Bonferroni's modification of Student's *t*-test. A *p* value below 0.05 was considered to indicate a statistically significant difference.

3. Results

The process of electrospinning using the Ti(IV) isopropoxide and PVP mixture produced flexible, roughly circular white meshes with an average diameter of 17 mm that were less than 1 mm in thickness. After calcination at 700 °C for 3 h, the meshes shrunk to an average diameter of 15 mm and became brittle. LCM images showed topographical differences between the two sides of the 6% PVP (Fig. 1a and b) and 10% PVP (Fig. 1c and d) TiO_2 meshes. The surface of the meshes that was exposed to the electrospinning setup was relatively flat, with fibers aligned randomly throughout the surface. In contrast, the surface of the mesh that was in contact with the cross-hatched bronze net used to collect the fibers retained the pattern stamped by the net, with bunches of aligned fibers forming ridges ranging from 13 to 26 μm in height. SEM images (Fig. 2a–d) and image analysis (Fig. 2e and f) revealed that the meshes were porous, with a similar average pore size of 1.44 ± 0.89 μm for 6% PVP scaffolds and 1.76 ± 1.00 μm for 10% PVP scaffolds. However, the higher-magnification SEM images (Fig. 2b and d) showed that changing the preparation from 6% to 10% PVP had an effect on the fiber diameter size, with the former having an average diameter of 184 ± 39 nm and the latter a significantly larger average diameter of 343 ± 98 nm.

LCM measurements (Table 1) revealed that the roughness of both the 6% and 10% scaffolds was similar, with their patterned side significantly rougher compared to the flat side. The XRD spectrum (Fig. 3) of the nanofiber TiO_2 meshes after calcination presented main peaks for rutile and anatase crystal structures in both PVP concentrations, with small differences in the intensity of the peaks. Chemical analysis by EDX (Table 2) showed that the initial PVP concentrations did not affect the final chemical composition after calcination, which included Ti and O as the major components with a molar ratio close to 1:2 consistent with the TiO_2 molecular formula. Small traces of Si and Ca were detected, but no C was found, in the EDX spectra of all the samples. The surface-sensitive XPS analysis (Table 3) also showed O and Ti as the main chemical species in both mesh groups, as well as the presence of C and Si in the spectra.

Cell morphology was similar on flat (Fig. 4) and patterned (Fig. 5) sides of the TiO_2 meshes, regardless of the percent of PVP used during processing. The cells grew throughout the surface with elongated morphology and in some cases seemed to grow along some of the ridges of the patterned side and into the largest pores of both of the meshes. The number of cells on the patterned P6% and P10% groups was similar, but lower than the cell number of flat groups (Fig. 6a). Cell numbers for all TiO_2 groups were lower than on TCPS. Alkaline phosphatase was affected in a similar manner,

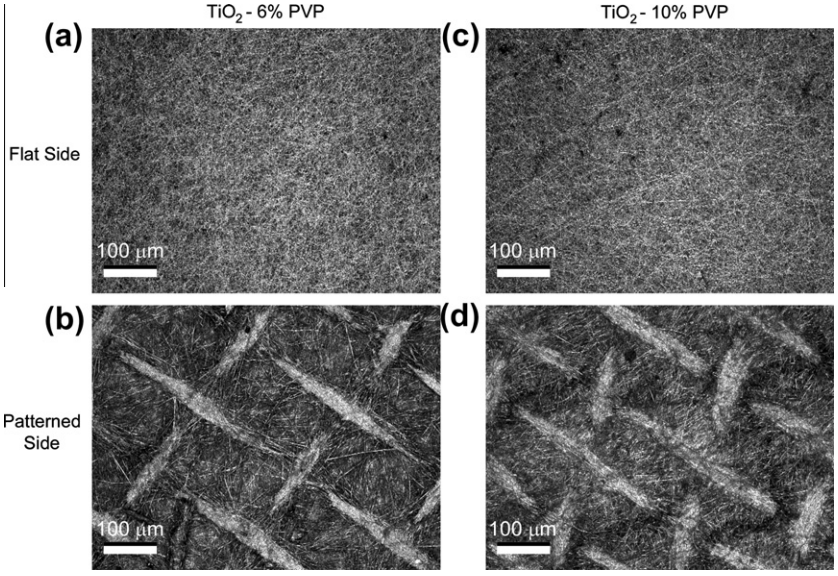

Fig. 1. LCM images of both flat and patterned sides of the TiO_2 meshes, made with 6% and 10% PVP. The nanofibers on the flat side of the meshes are randomly aligned, whereas the patterned side of the meshes has a clear cross-hatch pattern, with ridges of aligned nanofibers.

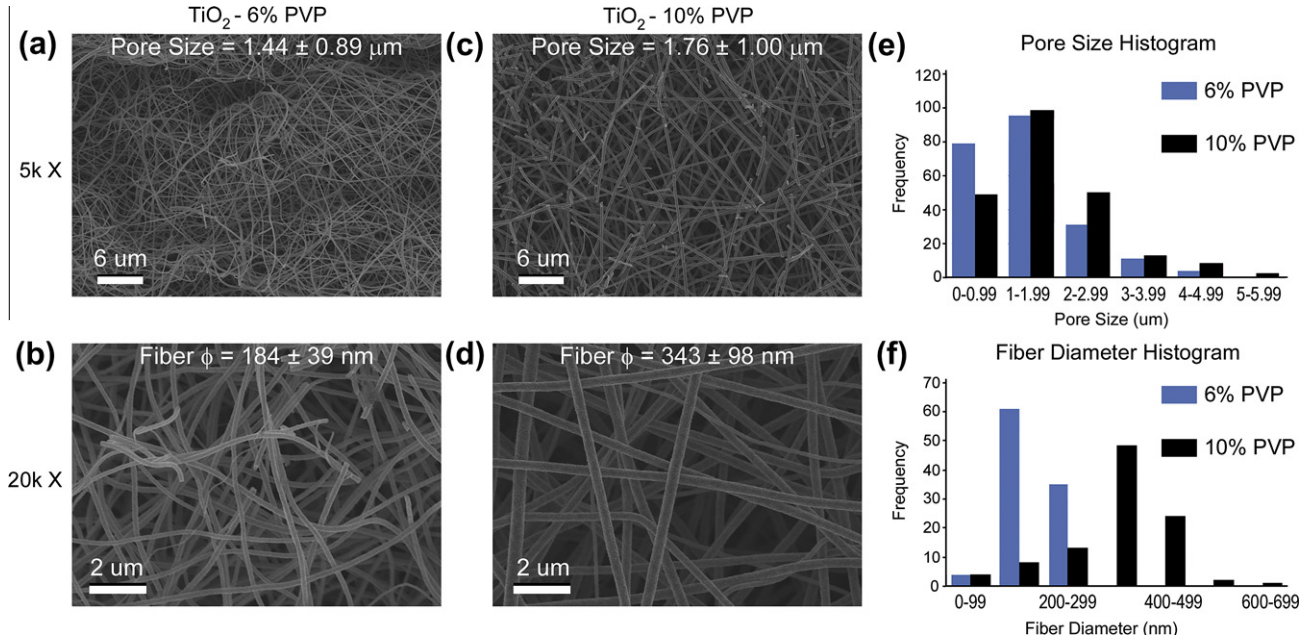

Fig. 2. SEM images and analysis of the morphology of the electrospun nanofiber TiO_2 meshes produced with (a,b) 6% or (c,d) 10% PVP. (e) Histograms at low magnification show similar pore sizes for both mesh formulations. However, (f) histograms at higher magnification reveal thinner nanofibers on the 6% PVP meshes compared to the 10% PVP.

Table 1
Surface roughness of TiO_2 meshes measured by LCM.

Sample	Surface roughness (S_a, mean ± SD) (μm)	Peak-to-peak height (S_z, mean ± SD) (μm)
TiO_2–6% PVP (flat)	0.57 ± 0.02	12.06 ± 3.33
TiO_2–6% PVP (patterned)	2.68 ± 0.35	53.00 ± 14.44
TiO_2–10% PVP (flat)	0.61 ± 0.05	25.11 ± 7.33
TiO_2–10% PVP (patterned)	2.15 ± 0.57	62.71 ± 8.79

with cells on the patterned side of the meshes having lower levels of enzyme activity than cells on the flat side, regardless of the PVP preparation (Fig. 6b). Osteocalcin levels were higher on the P10% group when compared to the F10% and P6% groups (Fig. 6c). Osteocalcin levels were also higher on all TiO_2 meshes compared to TCPS. Osteoprotegerin production was sensitive to both the micro-scale pattern of the surface and the size of the nano-fibers, as the levels were higher on the F10% group compared to F6%, and on both P6% and P10% groups compared to their flat sides (Fig. 6d). VEGF production was higher on P6% and P10% groups compared to TCPS, with P10% being significantly higher than its flat counterpart F10% (Fig. 6e).

4. Discussion

In this study the electrospinning process was used to create pure TiO_2 meshes that had the same chemical composition and crystal structure, but different surface roughness and nanofiber diameter. Differences in surface roughness were achieved by contrasting the side of each mesh that was exposed to the injection needle with the side that was in contact with the patterned bronze collector, resulting in a cross-hatch pattern.

LCM measurements confirmed the difference in roughness between the two sides of the meshes, and showed that the patterned side was comparatively rougher than the flat side. These results using inorganic fiber meshes support previous observations showing that different collector patterns affect the topography and fiber alignment of polymeric electrospun meshes [39,40].

By changing the PVP concentration of the starting solution from 6% to 10% PVP, the samples ended up with different average nanofiber diameters. These results are consistent with previous studies on electrospun titania meshes [41], which showed that properties such as fiber diameter and pore size are dependent on electrospinning parameters such as PVP and titanium precursor concentrations, electric field strength and solution feeding rate. Interestingly, these changes in surface roughness and fiber diameter were achieved without affecting the chemistry or the crystal structure of the substrates, thus emphasizing the effect of the structural variables of interest on cell response. In addition, the EDX results in combination with the lack of N in the XPS spectra supports the point that PVP was removed during calcination and the substrates are, indeed, mainly composed of TiO_2. However, the meshes became brittle after calcination, limiting their use for clinical applications. Our results are in agreement with other studies on similar meshes made with 7% PVP after calcination at 700 °C for 2 h that found no additional weight loss measured by thermogravimetric analysis [42]. The presence of C in the XPS spectra can be attributed to hydrocarbon and organic contamination, as has been well documented in studies of Ti/TiO_2 surfaces for implant applications when exposed to air [43,44]. The traces of Si in both the EDX and XPS spectra possibly come from contamination during calcination of the meshes on top of the Si wafers.

Cell morphology was not sensitive to differences in microscale structure or nanofiber diameter. However, cultures grew throughout the entire surface and interacted very closely with the nanofibers. No major effects on cell morphology were observed even on

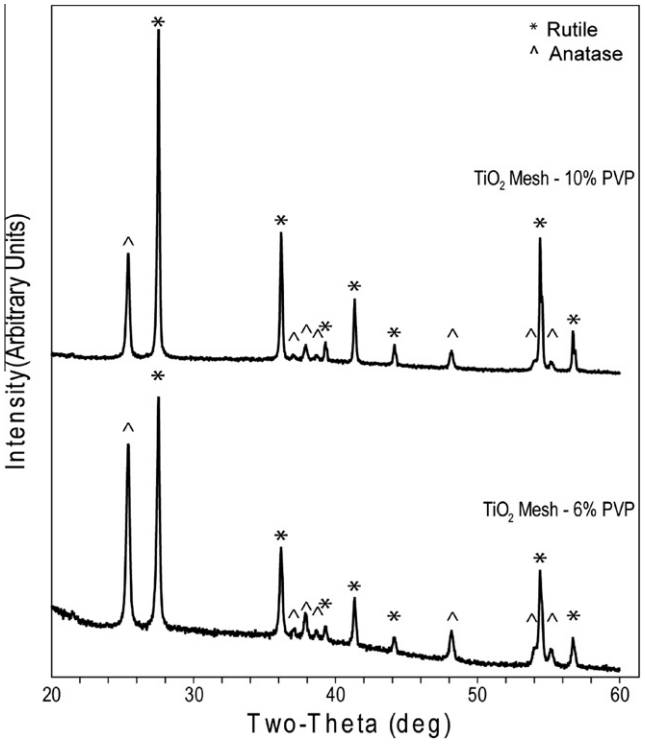

Fig. 3. XRD spectra of 6% and 10% TiO_2 nanofiber meshes.

Table 2
Elemental composition of TiO_2 meshes analyzed by EDX.

Sample	Concentration (mean at.% ± SD)			
	O	Ti	Si	Ca
TiO_2–6% PVP	72.5 ± 2.0	27.4 ± 2.1	0.3 ± 0.0	–
TiO_2–10% PVP	73.9 ± 1.0	25.7 ± 1.1	0.3 ± 0.0	0.2 ± 0.0

the samples imprinted with the cross-hatch pattern, although a few cells did align with some of the ridges. Previous studies on electrospun polymeric scaffolds reported preferential attachment of cells along patterned and aligned nanofibers during early culture time points, but not after cells reach a larger percentage of confluence [45–47]. It is possible that, during the earlier time points in our study, cell alignment with the ridges of the cross-hatch pattern might have been more evident, although this was not evaluated.

In the present study, the average pore size of the meshes was smaller than the size of the cells, so it was not possible for them to be incorporated into the mesh. However, cells still tried to migrate within the largest pores, as evidenced by single nanofibers covering parts of their cell extensions. Previously, non-woven electrospun scaffolds seeded with human mesenchymal stem cells (hMSC) have been shown to support cell growth, with even distribution inside the scaffolds after culture in a dynamic flow bioreactor, and to promote neovascularization within the scaffolds in a nude mouse subcutaneous model [48]. Conversely, it has recently been reported that most conventional electrospinning collecting systems result in tightly packed layers of nanofibers that hinder cell infiltration [49]. The same group developed a new "focused, low-density, uncompressed nanofiber" (FLUF) collection system that results in loosely packed scaffolds with large pores that allow improved infiltration of cells.

The cell number on the TiO_2 meshes was affected by the surface roughness of the samples and not necessarily by the size of the nanofibers. The rough side of both the 6% and 10% PVP meshes had lower cell numbers than their smooth side. The effect of surface roughness on cell number has been previously reported by our laboratory and others for Ti/TiO_2 surfaces that promote osteoblast differentiation [29,50–52]. The concept of decreased cell number on rougher surfaces that enhance osteoblast maturation has been explained as a transcriptionally regulated transition between cell proliferation and differentiation [53,54]. In contrast, other groups have found higher cell numbers with an increase in nanoroughness [55] or microroughness [56,57], or a combination of both [28]. Our results are also in agreement with other studies on electrospun polymeric scaffolds, which have found no effects on osteoblast proliferation due to nanofiber alignment [40,45] or nanofiber diameter [58].

Table 3
Surface elemental composition of TiO_2 meshes analyzed by XPS.

Sample	Concentration (mean at.% ± SD)			
	O	Ti	C	Si
TiO_2–6%PVP	61.1 ± 1.5	22.2 ± 2.0	11.8 ± 0.6	2.7 ± 1.2
TiO_2–10%PVP	63.7 ± 0.8	23.8 ± 0.8	8.94 ± 2.8	2.99 ± 2.2

Maturation of osteoblasts was controlled by a combination of surface roughness and fiber diameter on the TiO_2 meshes, i.e. a combination of microroughness and the nanotopography created by the nanofibers. Alkaline phosphatase specific activity, which is a marker of osteoblast differentiation expressed during early stages, was lower on the rough side of the 6% and 10% TiO_2 meshes and higher on the flat side of the 6% PVP meshes compared to TCPS. Osteocalcin, a late differentiation marker, was significantly higher on the rough side of 10% PVP meshes compared to all other groups, suggesting that osteoblasts were able to sense the combination of micro- and nanotopography, and thus differentiation was enhanced on these samples. Osteocalcin production was also dependent on the chemistry of the substrate, as levels on all TiO_2 meshes were higher than on TCPS. Many studies evaluating rough Ti/TiO_2 surfaces have reported enhanced differentiation, as evidenced by higher levels of alkaline phosphatase specific activity and osteocalcin compared to smooth surfaces, using MG63s [59] and hMSCs [22]. Our results are in agreement with other studies that have also found lower levels of alkaline phosphatase specific activity with associated higher production of osteocalcin on microrough surfaces [59,60] or combined micro- and nanorough surfaces that mimic bone structural hierarchy [29], suggesting a more mature osteoblastic phenotype. These results are attributed to the biphasic profile of alkaline phosphatase specific activity, with an earlier peak and subsequent down-regulation in production that precedes the step-like up-regulation of osteocalcin once the osteoblasts reach a certain stage of maturity [54]. Only few studies have looked at these differentiation markers on polymeric electrospun meshes, with no clear effect from either nanofiber alignment [45] or diameter [58].

The local factors OPG and VEGF were also sensitive to the combination of surface roughness and nanofiber diameter. OPG production was higher on the smooth side of the 10% meshes compared to the 6% meshes, favoring the larger nanofiber diameter on the flat substrates. However, the highest levels of OPG were found on the rough side of the 6% and 10% meshes. The highest levels of VEGF production were on the rough side of both meshes compared to TCPS, with the 10% PVP mesh also having higher levels compared to its smooth counterpart. Overall, our results show enhanced osteoblast maturation and local factor production on rougher TiO_2 porous meshes with a larger nanofiber diameter of around 340 nm (i.e. 10% PVP TiO_2 meshes). These results, together with the cell number, ALP and OCN data, suggest that the surface roughness of porous TiO_2 substrates, in combination with the nanotopography created by the fibers, can drive the maturation process of osteoblasts on these surfaces.

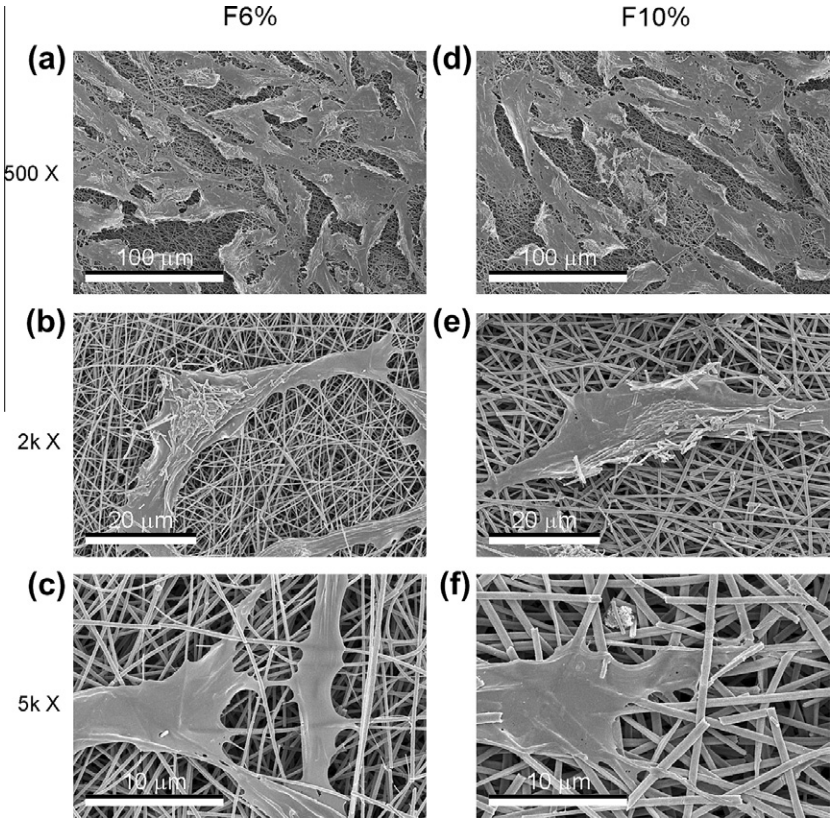

Fig. 4. SEM images at different magnifications of the morphology of MG63 osteoblast-like cells cultured on the flat side of the nanofiber TiO_2 meshes.

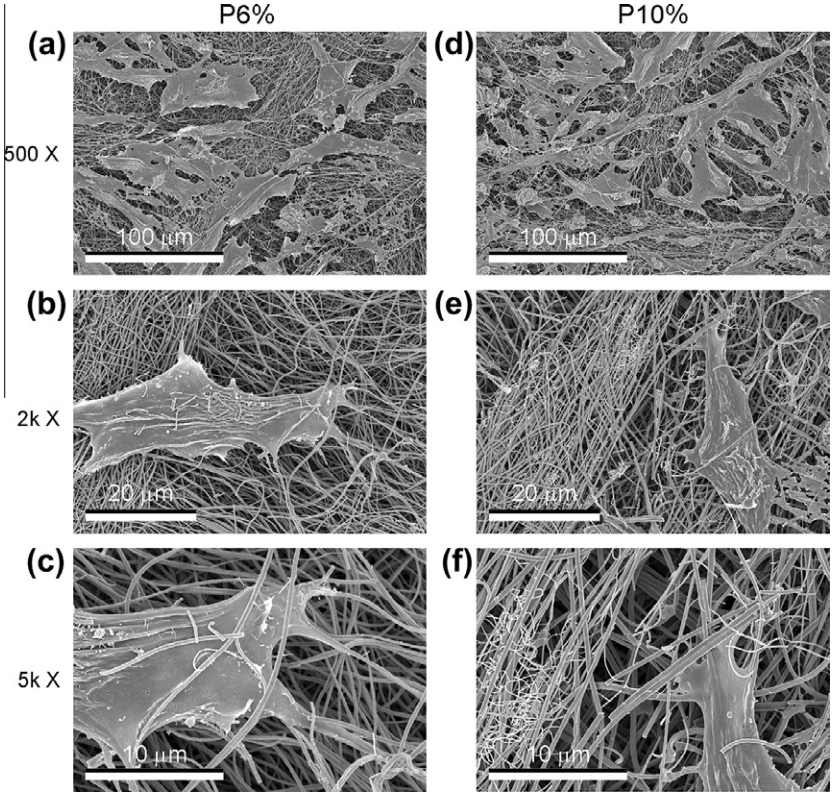

Fig. 5. SEM images at different magnifications of the morphology of MG63 osteoblast-like cells cultured on the patterned side of the nanofiber TiO_2 meshes.

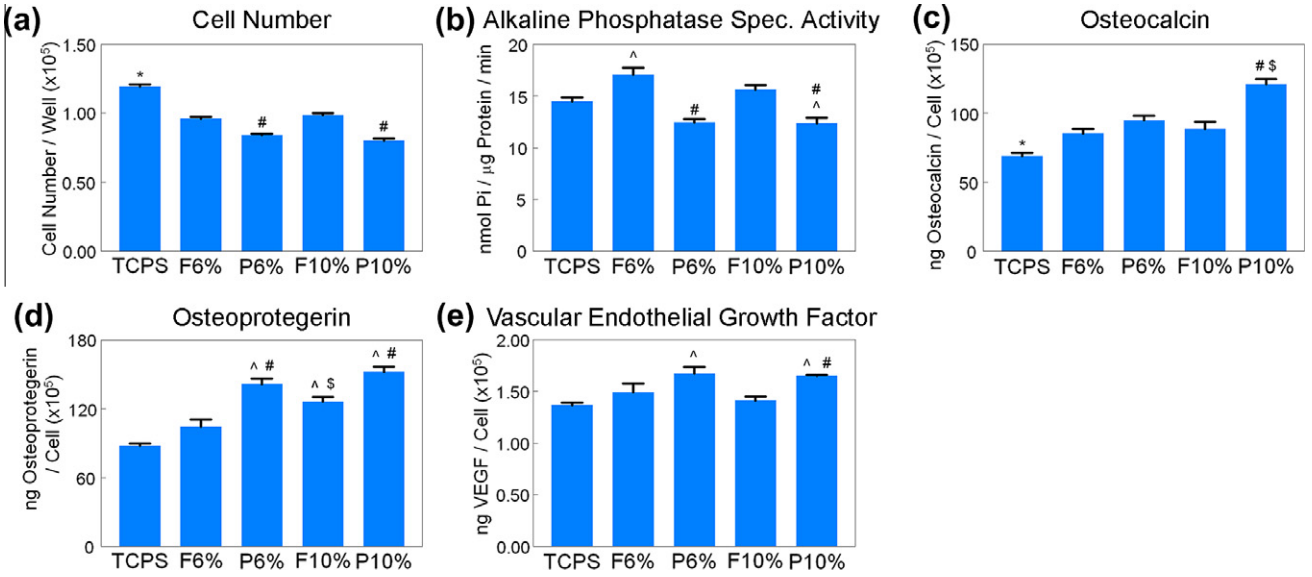

Fig. 6. Effects of structural properties of electrospun nanofiber TiO_2 meshes on osteoblast maturation. MG63 cells were plated on the flat or patterned side of both 6% and 10% PVP TiO_2 meshes and grown to confluence. At confluence, (a) cell number, (b) ALP specific activity, (c) OCN, (d) OPG and (e) VEGF levels were measured. Data represented are the mean ± SE of six independent samples. *Statistically significant p value below 0.05 vs. all TiO_2 groups; ^statistically significant p value below 0.05 vs. TCPS; #statistically significant p value below 0.05 vs. flat side of the same formulation; $statistically significant p value below 0.05 vs. 6% PVP of the same side.

5. Conclusion

In this study, we have evaluated the effect of porous and nanofiber TiO_2 meshes on the cell number, differentiation and local factor production of osteoblasts. The surface roughness and fiber diameter of the meshes could be varied without affecting their chemistry or crystal structure, emphasizing the effect of the structural parameters on cell response. The different TiO_2 mesh groups supported osteoblast viability, as the cells grew throughout the entire surfaces. The TiO_2 chemistry seemed to enhance osteoblast maturation, as all experimental groups had lower cell numbers and higher levels of differentiation markers compared to TCPS. Although cell morphology was similar on all TiO_2 mesh groups, cell response was sensitive to the substrate. Moreover, cell number, differentiation and local factor production were regulated by different structural aspects of the meshes. The final cell number of osteoblasts was controlled by the surface microroughness, whereas differentiation and local factor production were affected by both surface microscale pattern and nanofiber diameter, indicating that osteoblasts are sensitive to both microroughness and the nanotopography created by the TiO_2 nanofibers. Finally, the combination of microroughness with the nanotopography created by the larger nanofibers enhanced osteoblast differentiation and local factor production, indicating that there might be a lower-limit threshold in the size of the nanofibers that could be sensed by the osteoblasts to differentiate and generate an osteogenic environment. In conclusion, inorganic scaffold structural cues alone can be used to drive cell differentiation and create an osteogenic environment without the use of exogenous factors, thus structural parameters should be carefully considered when designing a scaffold for tissue engineering applications.

Acknowledgements

This research was supported by USPHS AR052102 and the Wallace H. Coulter Foundation. R.A.G. is partially supported by a fellowship from IFARHU-SENACYT. H.C. is grateful for support from the Ministry of Science and Technology of China (Grants 2011AA030102 and 2012CB933903).

Appendix A. Supplementary data

Supplementary data associated with this article can be found, in the online version, at doi:10.1016/j.actbio.2011.10.023.

Appendix B. Figures with essential colour discrimination

Certain figure in this article, particularly Figures 2 and 6, is difficult to interpret in black and white. The full colour images can be found in the on-line version, at doi:10.1016/j.actbio.2011.10.023.

References

[1] Jacobs JJ, Andersson GBJ, Bell JE, Weinstein SL, Dormans JP, Gnatz SM, et al. The burden of musculoskeletal diseases in the United States. Rosemont, IL: AAOS; 2008.
[2] Agrawal CM, Attawia M, Borden MD, Boyan BD, Bruder SP, Bucholz RW, et al. Bone graft substitutes. Rosemont, IL: ASTM–AAOS; 2003.
[3] Hing KA. Bioceramic bone graft substitutes: influence of porosity and chemistry. Int J Appl Ceram Technol 2005;2:184–99.
[4] Lutolf MP, Hubbell JA. Synthetic biomaterials as instructive extracellular microenvironments for morphogenesis in tissue engineering. Nat Biotechnol 2005;23:47–55.
[5] Heijkants RGJC, Van Tienen TG, De Groot JH, Pennings AJ, Buma P, Veth RPH, et al. Preparation of a polyurethane scaffold for tissue engineering made by a combination of salt leaching and freeze-drying of dioxane. J Mater Sci 2006;41:2423–8.
[6] Miao XG, Tan DM, Li J, Xiao Y, Crawford R. Mechanical and biological properties of hydroxyapatite/tricalcium phosphate scaffolds coated with poly(lactic-co-glycolic acid). Acta Biomater 2008;4:638–45.
[7] Sill TJ, von Recum HA. Electro spinning: applications in drug delivery and tissue engineering. Biomaterials 2008;29:1989–2006.
[8] Huang ZM, Zhang YZ, Kotaki M, Ramakrishna S. A review on polymer nanofibers by electrospinning and their applications in nanocomposites. Compos Sci Technol 2003;63:2223–53.
[9] Stitzel J, Liu J, Lee SJ, Komura M, Berry J, Soker S, et al. Controlled fabrication of a biological vascular substitute. Biomaterials 2006;27:1088–94.
[10] McManus M, Boland E, Sell S, Bowen W, Koo H, Simpson D, et al. Electrospun nanofibre fibrinogen for urinary tract tissue reconstruction. Biomed Mater 2007;2:257–62.
[11] Venugopal JR, Low S, Choon AT, Kumar AB, Ramakrishna S. Nanobioengineered electrospun composite nanofibers and osteoblasts for bone regeneration. Artif Organs 2008;32:388–97.
[12] Yoshimoto H, Shin YM, Terai H, Vacanti JP. A biodegradable nanofiber scaffold by electrospinning and its potential for bone tissue engineering. Biomaterials 2003;24:2077–82.

[13] Li WJ, Laurencin CT, Caterson EJ, Tuan RS, Ko FK. Electrospun nanofibrous structure: a novel scaffold for tissue engineering. J Biomed Mater Res 2002;60:613–21.
[14] Matthews JA, Wnek GE, Simpson DG, Bowlin GL. Electrospinning of collagen nanofibers. Biomacromolecules 2002;3:232–8.
[15] Jin HJ, Chen JS, Karageorgiou V, Altman GH, Kaplan DL. Human bone marrow stromal cell responses on electrospun silk fibroin mats. Biomaterials 2004;25:1039–47.
[16] Bhattarai N, Edmondson D, Veiseh O, Matsen FA, Zhang MQ. Electrospun chitosan-based nanofibers and their cellular compatibility. Biomaterials 2005;26:6176–84.
[17] Zhang YZ, Ouyang HW, Lim CT, Ramakrishna S, Huang ZM. Electrospinning of gelatin fibers and gelatin/PCL composite fibrous scaffolds. J Biomed Mater Res B Appl Biomater 2005;72B:156–65.
[18] Wagner WR, Hong Y, Huber A, Takanari K, Amoroso NJ, Hashizume R, et al. Mechanical properties and in vivo behavior of a biodegradable synthetic polymer microfiber–extracellular matrix hydrogel biohybrid scaffold. Biomaterials 2011;32:3387–94.
[19] Li CM, Vepari C, Jin HJ, Kim HJ, Kaplan DL. Electrospun silk–BMP-2 scaffolds for bone tissue engineering. Biomaterials 2006;27:3115–24.
[20] Gao Y, Cao WL, Wang XY, Gong YD, Tian JM, Zhao NM, et al. Characterization and osteoblast-like cell compatibility of porous scaffolds: bovine hydroxyapatite and novel hydroxyapatite artificial bone. J Mater Sci Mater Med 2006;17:815–23.
[21] Stein GS, Zhang Y, Hassan MQ, Li ZY, Stein JL, Lian JB, et al. Intricate gene regulatory networks of helix–loop–helix (HLH) proteins support regulation of bone-tissue related genes during osteoblast differentiation. J Cell Biochem 2008;105:487–96.
[22] Olivares-Navarrete R, Hyzy SL, Hutton DL, Erdman CP, Wieland M, Boyan BD, et al. Direct and indirect effects of microstructured titanium substrates on the induction of mesenchymal stem cell differentiation towards the osteoblast lineage. Biomaterials 2010;31:2728–35.
[23] Mendonca G, Mendonca DBS, Aragao FJL, Cooper LF. Advancing dental implant surface technology – from micron- to nanotopography. Biomaterials 2008;29:3822–35.
[24] Mendonca G, Mendonca DBS, Simoes LGP, Araujo AL, Leite ER, Duarte WR, et al. The effects of implant surface nanoscale features on osteoblast-specific gene expression. Biomaterials 2009;30:4053–62.
[25] Biggs MJP, Richards RG, Dalby MJ. Nanotopographical modification: a regulator of cellular function through focal adhesions. Nanomedicine 2010;6:619–33.
[26] Curtis ASG, Gadegaard N, Dalby MJ, Riehle MO, Wilkinson CDW, Aitchison G. Cells react to nanoscale order and symmetry in their surroundings. IEEE Trans NanoBiosci 2004;3:61–5.
[27] Mendonca G, Mendonca DBS, Aragao FJL, Cooper LF. The combination of micron and nanotopography by H_2SO_4/H_2O_2 treatment and its effects on osteoblast-specific gene expression of hMSCs. J Biomed Mater Res A 2010;94A:169–79.
[28] Kubo K, Tsukimura N, Iwasa F, Ueno T, Saruwatari L, Aita H, et al. Cellular behavior on TiO_2 nanonodular structures in a micro-to-nanoscale hierarchy model. Biomaterials 2009;30:5319–29.
[29] Gittens RA, McLachlan T, Olivares-Navarrete R, Cai Y, Berner S, Tannenbaum R, et al. The effects of combined micron-/submicron-scale surface roughness and nanoscale features on cell proliferation and differentiation. Biomaterials 2011;32:3395–403.
[30] Franceschi RT, James WM, Zerlauth G. 1-Alpha,25-dihydroxyvitamin-D3 specific regulation of growth, morphology, and fibronectin in a human osteo-sarcoma cell-line. J Cell Physiol 1985;123:401–9.
[31] Lajeunesse D, Kiebzak GM, Frondoza C, Sacktor B. Regulation of osteocalcin secretion by human primary bone-cells and by the human osteosarcoma cell-line Mg-63. Bone Miner 1991;14:237–50.
[32] Kieswetter K, Schwartz Z, Hummert TW, Cochran DL, Simpson J, Dean DD, et al. Surface roughness modulates the local production of growth factors and cytokines by osteoblast-like MG-63 cells. J Biomed Mater Res 1996;32:55–63.
[33] Bretaudiere JP, Spillman T. Alkaline Phosphatases. Weinheim: Verlag Chemica; 1984.
[34] Martin JY, Schwartz Z, Hummert TW, Schraub DM, Simpson J, Lankford J, et al. Effect of titanium surface-roughness on proliferation, differentiation, and protein-synthesis of human osteoblast-like cells (mg63). J Biomed Mater Res 1995;29:389–401.
[35] Smith PK, Krohn RI, Hermanson GT, Mallia AK, Gartner FH, Provenzano MD, et al. Measurement of protein using bicinchoninic acid. Anal Biochem 1985;150:76–85.
[36] Gundberg CM, Hauschka PV, Lian JB, Gallop PM. Osteocalcin – isolation, characterization, and detection. Methods Enzymol 1984;107:516–44.
[37] Simonet WS, Lacey DL, Dunstan CR, Kelley M, Chang MS, Luthy R, et al. Osteoprotegerin: a novel secreted protein involved in the regulation of bone density. Cell 1997;89:309–19.
[38] Raines AL, Olivares-Navarrete R, Wieland M, Cochran DL, Schwartz Z, Boyan BD. Regulation of angiogenesis during osseointegration by titanium surface microstructure and energy. Biomaterials 2010;31:4909–17.
[39] Li D, Ouyang G, McCann JT, Xia YN. Collecting electrospun nanofibers with patterned electrodes. Nano Lett 2005;5:913–6.
[40] Wang YZ, Wang GX, Chen L, Li H, Yin TY, Wang BC, et al. Electrospun nanofiber meshes with tailored architectures and patterns as potential tissue-engineering scaffolds. Biofabrication 2009;1.
[41] Li D, Xia YN. Fabrication of titania nanofibers by electrospinning. Nano Lett 2003;3:555–60.
[42] Park S-J, Chase GG, Jeong K-U, Kim HY. Mechanical properties of titania nanofiber mats fabricated by electrospinning of sol–gel precursor. J Sol–Gel Sci Technol 2010;54:188–94.
[43] Rupp F, Scheideler L, Olshanska N, deWild M, Wieland M, Geis-Gerstorfer J. Enhancing surface free energy and hydrophilicity through chemical modification of microstructured titanium implant surfaces. J Biomed Mater Res A 2006;76A:323–34.
[44] Massaro C, Rotolo P, De Riccardis F, Milella E, Napoli A, Wieland M, et al. Comparative investigation of the surface properties of commercial titanium dental implants. Part I. Chemical composition. J Mater Sci Mater Med 2002;13:535–48.
[45] Ma J, He X, Jabbari E. Osteogenic differentiation of marrow stromal cells on random and aligned electrospun poly(l-lactide) nanofibers. Ann Biomed Eng 2010;39:14–25.
[46] Meinel AJ, Kubow KE, Klotzsch E, Garcia-Fuentes M, Smith ML, Vogel V, et al. Optimization strategies for electrospun silk fibroin tissue engineering scaffolds. Biomaterials 2009;30:3058–67.
[47] Murugan R, Ramakrishna S. Design strategies of tissue engineering scaffolds with controlled fiber orientation. Tissue eng 2007;13:1845–66.
[48] Srouji S, Kizhner T, Suss-Tobi E, Livne E, Zussman E. 3-D nanofibrous electrospun multilayered construct is an alternative ECM mimicking scaffold. J Mater Sci Mater Med 2008;19:1249–55.
[49] Blakeney BA, Tambralli A, Anderson JM, Andukuri A, Lim D-J, Dean DR, et al. Cell infiltration and growth in a low density, uncompressed three-dimensional electrospun nanofibrous scaffold. Biomaterials 2011;32:1583–90.
[50] Wall I, Donos N, Carlqvist K, Jones F, Brett P. Modified titanium surfaces promote accelerated osteogenic differentiation of mesenchymal stromal cells in vitro. Bone 2009;45:17–26.
[51] Zhao G, Zinger O, Schwartz Z, Wieland M, Landolt D, Boyan BD. Osteoblast-like cells are sensitive to submicron-scale surface structure. Clin Oral Implants Res 2006;17:258–64.
[52] Kim MJ, Kim CW, Lim YJ, Heo SJ. Microrough titanium surface affects biologic response in MG63 osteoblast-like cells. J Biomed Mater Res A 2006;79:1023–32.
[53] Stein GS, Lian JB, Stein JL, VanWijnen AJ, Montecino M. Transcriptional control of osteoblast growth and differentiation. Physiol Rev 1996;76:593–629.
[54] Lian JB, Stein GS. Concepts of osteoblast growth and differentiation – basis for modulation of bone cell-development and tissue formation. Crit Rev Oral Biol Med 1992;3:269–305.
[55] Han P, Ji WP, Zhao CL, Zhang XN, Jiang Y. Improved osteoblast proliferation, differentiation and mineralization on nanophase Ti6Al4V. Chin Med J (Engl) 2011;124:273–9.
[56] Kubies D, Himmlova L, Riedel T, Chanova E, Balik K, Douderova M, et al. The interaction of osteoblasts with bone-implant materials. 1. The effect of physicochemical surface properties of implant materials. Physiol Res 2011;60:95–111.
[57] Brett PM, Harle J, Salih V, Mihoc R, Olsen I, Jones FH, et al. Roughness response genes in osteoblasts. Bone 2004;35:124–33.
[58] Badami A, Kreke M, Thompson M, Riffle J, Goldstein A. Effect of fiber diameter on spreading, proliferation, and differentiation of osteoblastic cells on electrospun poly(lactic acid) substrates. Biomaterials 2006;27:596–606.
[59] Zinger O, Zhao G, Schwartz Z, Simpson J, Wieland M, Landolt D, et al. Differential regulation of osteoblasts by substrate microstructural features. Biomaterials 2005;26:1837–47.
[60] Zhao G, Raines AL, Wieland M, Schwartz Z, Boyan BD. Requirement for both micron- and submicron scale structure for synergistic responses of osteoblasts to substrate surface energy and topography. Biomaterials 2007;28:2821–9.